Materials Letters 254 (2019) 33–36

Contents lists available at ScienceDirect

Materials Letters

journal homepage: www.elsevier.com/locate/mlblue

# Selective laser melted $TiB_2$/Ti6Al4V graded materials and first-principle calculations

Rui Wang [a,b], Dongdong Gu [a,b,*], Lixia Xi [a,b], Kaijie Lin [a,b], Meng Guo [a,b], Hongmei Zhang [a,b]

[a] College of Materials Science and Technology, Nanjing University of Aeronautics and Astronautics, Yudao Street 29, Nanjing 210016, Jiangsu Province, PR China
[b] Jiangsu Provincial Engineering Laboratory for Laser Additive Manufacturing of High-Performance Metallic Components, Nanjing University of Aeronautics and Astronautics, Yudao Street 29, Nanjing 210016, Jiangsu Province, PR China

ARTICLE INFO

*Article history:*
Received 14 May 2019
Received in revised form 23 June 2019
Accepted 4 July 2019
Available online 5 July 2019

*Keywords:*
Selective laser melting
Interfaces
Microstructure
Graded materials
First-principle calculations

ABSTRACT

Selective laser melting (SLM), as a rapidly developed layer-by-layer 3D printing technology, has been demonstrated that it can be used for additive manufacturing of multi-materials. In this work, $TiB_2$/Ti6Al4V multi-materials were manufactured by SLM. The results showed that interfacial microstructures consisting of un-melted $TiB_2$ powders, columnar TiB crystals, and acicular TiB crystals were formed in the molten pool. Meanwhile, a variation nanohardness was developed with chemical compositions at the interfacial regions, owing to an in-situ reaction of Ti and $TiB_2$. The first-principle calculations were used to reveal the axial growth of TiB crystals as well as the different hardness of this system.



## 1. Introduction

Selective laser melting (SLM), as a rapidly developed layer by layer additive manufacturing technique, is capable to produce high densification and complex parts by using of metal, ceramic, or composite materials [1,2]. For many practical engineering applications, multi-materials SLM is indispensable due to the requirement of different material properties at different regions. Tan et al. have clearly revealed the feasibility of combining different metals with good metallurgical bonding using SLM [3]. Compared with metal-metal multiple materials, there are more challenges for SLM of metal-ceramic multiple materials. These are involved with the extremely different bond strength and thermal expansion coefficient between metal and ceramic, leading to thermal stress and even delamination during non-equilibrium solidification of SLM [4].

To overcome the above constraints, fabrication of functional graded materials (FGM) through good interfacial bonding between metal and ceramic is feasible. This method can avoid residual stress concentration and fracture propagation by reducing the saltation of different properties between neighboring layers [5,6]. Shishkovsky et al. [7] have successfully fabricated functional graded specimens and realized a hardness gradient via SLM using the compositionally grade powders (Ti+(10, 15 or 20 vol.%) $TiB_2$). The nanohardness of SLMed Ti6Al4V with 3 wt% $TiB_2$ can reach to 6.00 GPa due to the reinforcement effect of needle-like TiB [8]. Nevertheless, it is difficult to make a larger range of hardness difference for multi-materials SLM of pure $TiB_2$ and Ti6Al4V powders instead of composite powders. Interfacial reaction and microstructure are vital to the connection characteristic of adjacent layers. In this work, graded materials were prepared by SLM of $TiB_2$/Ti6Al4V multi-materials. The microstructure and nanohardness at the interface were investigated. Additionally, first-principle calculations were used to explain the axial growth of TiB and different hardness of this system.

## 2. Materials and methods

The SLM equipment was composed of an IPG YLR-500 Ytterbium fiber laser with a 1070 ± 10 nm wavelength. Fig. 1a shows the SLM process of Ti6Al4V and $TiB_2$ powders. Cubic samples were fabricated layer by layer on a Ti6Al4V substrate. Based on our previous research [9], the laser power ($P$), scanning speed ($v$) and hatch spacing of Ti6Al4V layer were 250 W, 600 mm/s, and 50 μm, respectively. While for the $TiB_2$ layer, the respective laser scanning speed and hatch spacing were set as 80 mm/s and 120 μm. The laser power varied from 200 W to 500 W with an interval of 50 W. The starting powders of Ti6Al4V (99.7% purity,

* Corresponding author at: College of Materials Science and Technology, Nanjing University of Aeronautics and Astronautics, Yudao Street 29, Nanjing 210016, Jiangsu Province, PR China.
*E-mail address:* dongdonggu@nuaa.edu.cn (D. Gu).

https://doi.org/10.1016/j.matlet.2019.07.015
0167-577X/

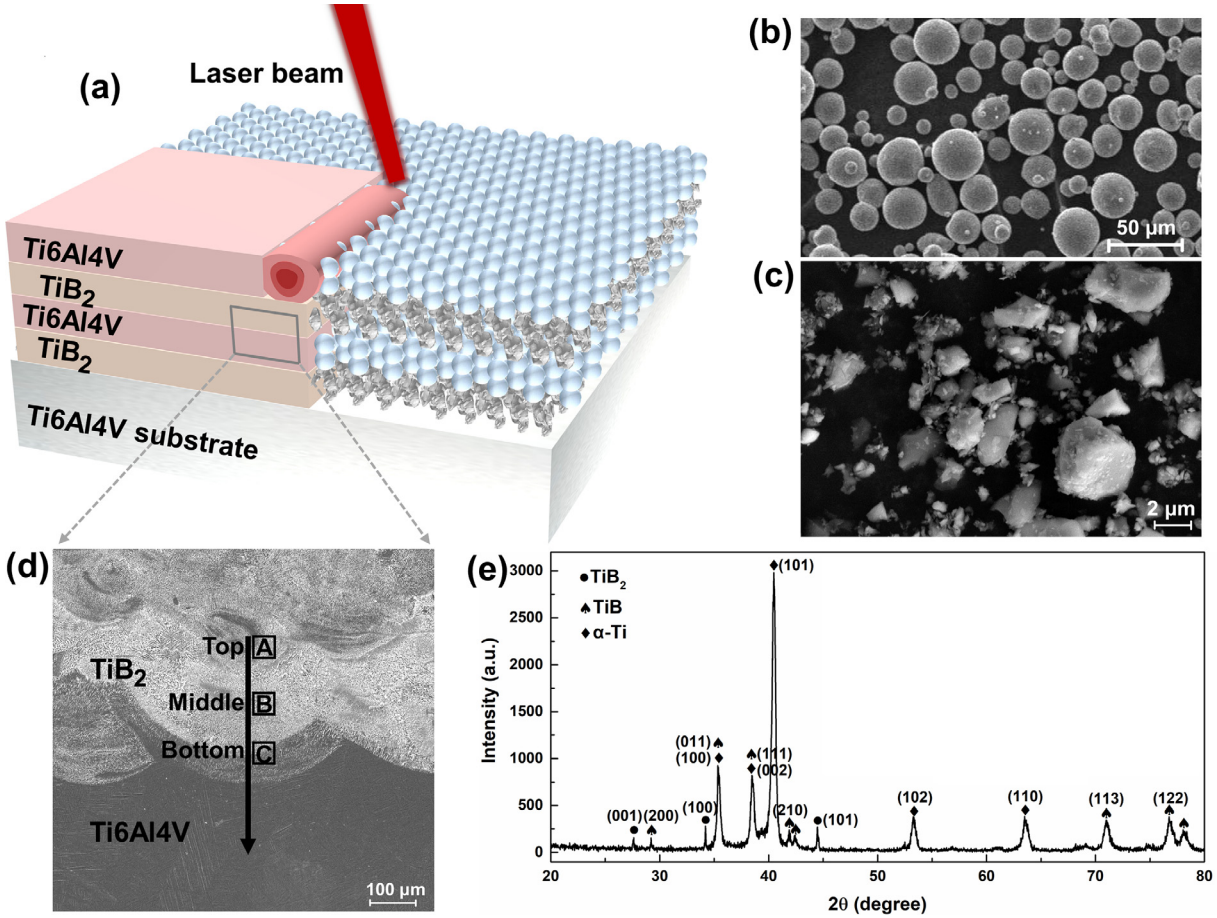


**Fig. 1.** (a) Schematic of SLM process with $TiB_2$/Ti6Al4V multi-materials; FE-SEM images of (b) $TiB_2$ and (c) Ti6Al4V powders; (d) cross-section of SLMed $TiB_2$/Ti6Al4V multi-materials under $v$ = 80 mm/s, $P$ = 400 W; (e) XRD pattern of SLMed TiB2/Ti6Al4V multi-materials taken from the interface.

$D_{50}$: 24.06 μm) with a spherical shape and $TiB_2$ (98.9% purity, $D_{50}$: 2.21 μm) with an irregular shape are shown in Fig. 1b and c.

Phase identification was studied by X-ray diffraction (XRD, Cu Kα). Microstructures were characterized by field emission scanning electron microscope (FE-SEM, Hitachi, Japan). The chemical compositions were determined by an energy dispersive spectrometer (EDS). Besides, nanohardness test was measured on the polished samples with a force of 20 mN and holding time of 10 s by a nanoindentation tester (Agilent Nano Indenter G200, USA). The first-principle calculations were performed using the VASP code. Considering the occurrence of α-Ti in SLM-processed Ti6Al4V samples [8], crystal structure of pure Ti crystal was used to simplify the complex crystal of Ti6Al4V.

## 3. Results and discussion

For a low laser power of 200 W and 250 W, many pores appeared at the cross-section of SLM-processed $TiB_2$/Ti6Al4V multi-materials under $v$ of 80 mm/s. As the laser power increased to 350 W, samples with good interfacial bonding were obtained because of enough energy input. Hence, the SLM-processed sample at a laser power of 400 W was taken as an example to investigate interfacial microstructure and property (Fig. 1d). The XRD pattern of sample taken from the interface showed the presence of α-Ti, TiB and $TiB_2$ diffraction peaks (Fig. 1e). Recent researches on $TiB_2$ reinforced Ti6Al4V composites illustrated that reaction between Ti and $TiB_2$ can proceed as follows: $Ti + TiB_2 = 2TiB$ [8,10], that is to say, TiB can be formed by an reaction of Ti and $TiB_2$ under high laser radiation. This explains the appearance of TiB phase in the SLM-processed samples.

Fig. 2a shows the SEM micrographs of three different regions in molten pool: Top (A), middle (B), and bottom (C) as shown in Fig. 1d. From Fig. 2b, it can be found that the atomic ratio of Ti and B at point 1 is 1:2. It means that in the region A, a small amount of $TiB_2$ particles remained in an irregular shape are consistent with the weak $TiB_2$ peaks of XRD pattern. Columnar and fine acicular crystals were observed in the middle and bottom of molten pool, respectively. An atom ratio of Ti and B with 1:1 for points 2 and 3 has proved to be TiB crystals. The different diameters of TiB crystals are caused by a large temperature gradient and different cooling rate during high-power laser melting. Finer crystal is obtained from the bottom of melten pool with higher cooling rates, attributed to shorter growth time of crystal. In addition, the temperature is the highest at the pool center and decreases gradually with distance away from the center. Thus, the columnar crystals in the region A with lower cooling rate, the acicular crystals in the region B with higher cooling rate and un-melted $TiB_2$ in the region C with lower temperature can be observed. From the Fig. 2b and c, it can be seen that Al and V elements also existed in the top and middle of the molten pool, which indicated that elements of Ti, Al, and V could diffuse into the interface. Considering the α-Ti generated during laser melting of Ti6Al4V [8], TiB crystals can be produced by a chemical reaction of Ti with $TiB_2$ at the interface, which led to the formation of gradient interface between the $TiB_2$ and Ti6Al4V. Based on the results of EDS line scanning, the content of B in the top of molten pool was obviously high at a

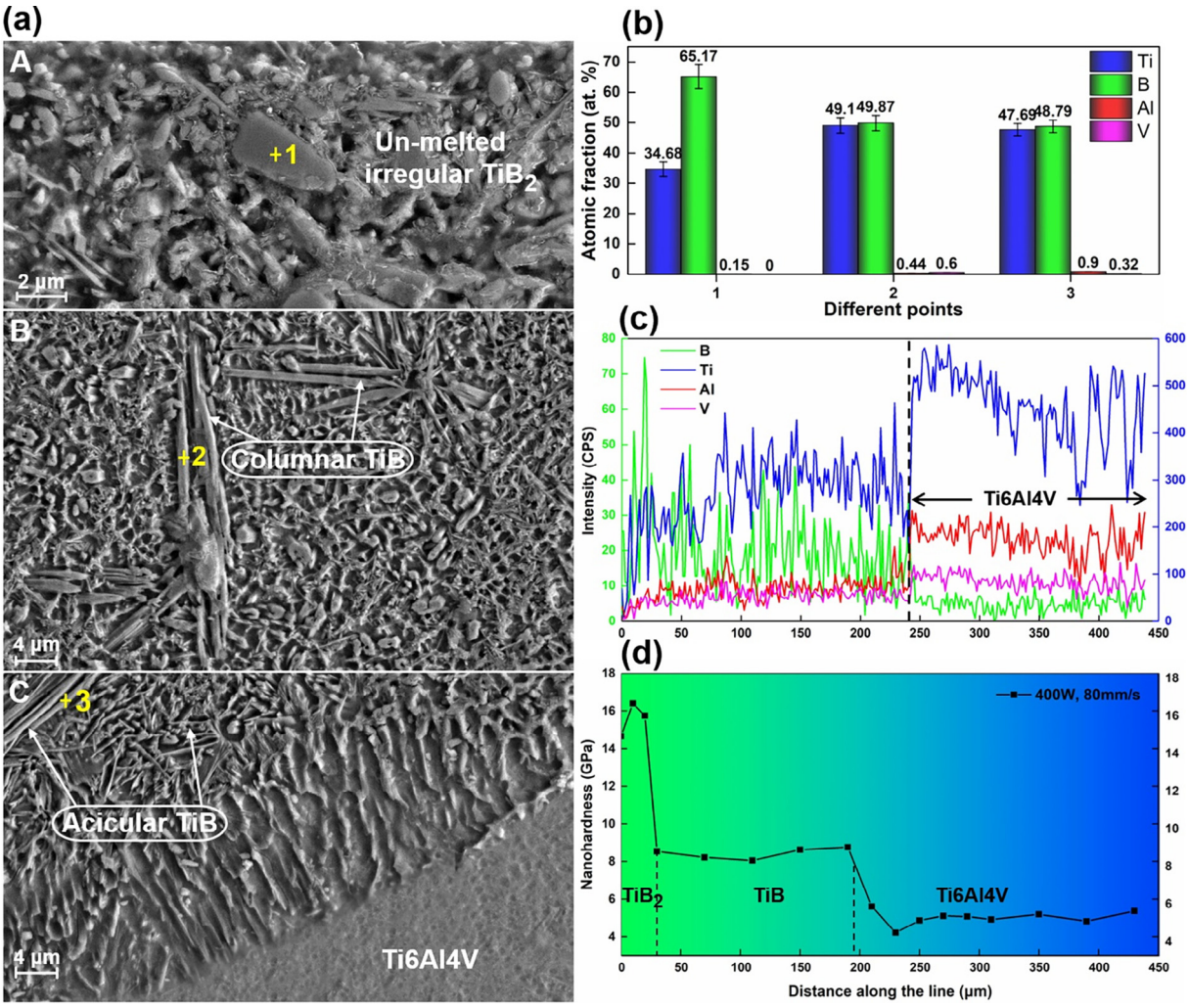


**Fig. 2.** (a) FE-SEM micrographs showing the different regions of A, B and C of the molten pool in Fig. 1d; (b) chemical compositions by EDS analysis: atomic fraction of Ti, B, Al and V elements at three different positions in Fig. 2a; (c) EDS line-scan analysis and (d) nanoindentation along the line in Fig. 1d.

depth of 0–30 μm and its content gradually stabilized at about 30–240 μm, then started to decline. This suggests that boron diffusion is hard to traverse the pool boundary into Ti6Al4V. However, the increasing intensity of Ti, Al, V at a depth of 250 μm indicate the reaching of Ti6Al4V layer. In general, the TiB crystals in the transition region alleviate the residual stress due to gradient compositions.

Nanohardness measurements were conducted on the interfacial region of $TiB_2$/Ti6Al4V and the results are shown in Fig. 2d. Nanohardness with an approximate value of 4.8 GPa for Ti6Al4V layer is comparable to reported values [11,12]. According to the gradient change of nanohardness across the interfacial region, it is noted that TiB makes a good transition between the $TiB_2$ and Ti alloy. Therefore, $TiB_2$/TiB/Ti6Al4V graded materials promote the formation of good bonding between dissimilar materials. This graded materials additive manufacturing is beneficial to combine the hard ceramic with ductile metal into an organic whole effectively.

The theoretical calculations were performed to investigate the physical origins of different hardness between $TiB_2$, TiB, and Ti6Al4V. Fig. 3a shows that α-Ti are composed of metallic bond ($d_{Ti\text{-}Ti}$ = 2.86 Å). From the supercell, both TiB and $TiB_2$ are mainly consisted of B-B covalent bonds, and the covalent bond length of TiB ($d_{B\text{-}B}$ = 1.81 Å) is larger than $TiB_2$ ($d_{B\text{-}B}$ = 1.75 Å). Therefore, the covalency of TiB is weaker than that of $TiB_2$. As the hardness of a material is a reflection of the internal bonding strength, and the impacts of several chemical bonds are covalent bond > ionic bond > metal bond. Thus, the hardness order of these three materials is $TiB_2$ > TiB > Ti (Ti6Al4V). Apart from the crystal structure calculation, the electronic structure has been also studied. The charge distributions of TiB and $TiB_2$ are shown in Fig. 3b, zigzag chain of TiB and hexagonal network structure of $TiB_2$ demonstrate the delocalized π-bonds between the boron atoms. In this situation, TiB structure characterized by zigzag chains of boron atoms is parallel to the [0 1 0] direction, this anisotropic crystal structure may be responsible for an axial growth as observed in Fig. 2a. From Fig. 3c, it can be seen that α-Ti exhibits a good metallicity due to local electronic density of states around the fermi level. The electronic structures of both TiB and $TiB_2$ are governed by the strong hybridization between the Ti-3*d* and B-2*p* states. In particular, the appearance of the pseudo-gap (yellow region) around the fermi level also lead to increased stability of $TiB_2$. Therefore, the structure stability is in an order of $TiB_2$ > TiB > Ti6Al4V. Hardness and elasticity of these materials with distinct bonding may show a similar gradient tendency, which contributes to less residual stress and good interfacial bonding.

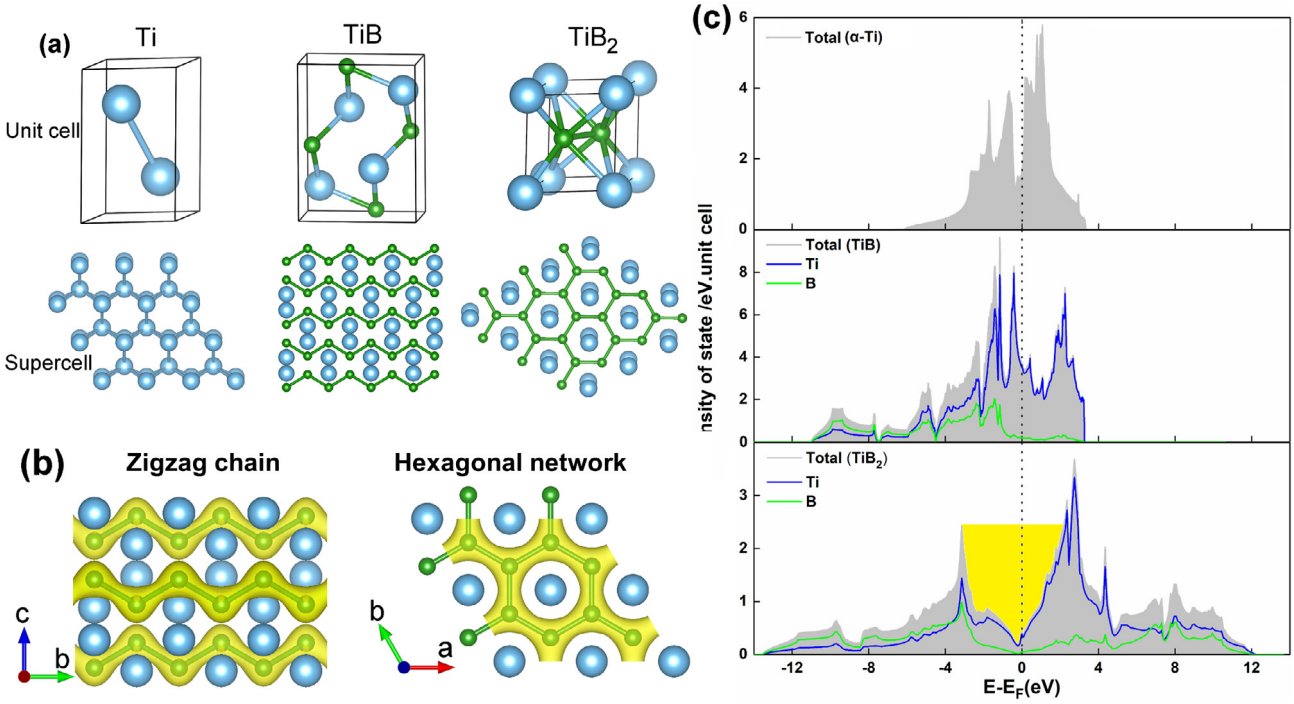


**Fig. 3.** (a) Unit cell and supercell of Ti, TiB and $TiB_2$; (b) charge distribution of TiB and $TiB_2$; (c) partial density of states of the system.

## 4. Conclusions

$TiB_2$/TiB/Ti6Al4V graded materials have been achieved by SLM of $TiB_2$/Ti6Al4V multi-materials. TiB was formed by an in-situ reaction of Ti with $TiB_2$ and the gradual variations of chemical compositions caused a variation in nanohardness along the interface. The structural stabilities of $TiB_2$, TiB, and Ti6Al4V were also studied by first-principle calculations. The hardness gradient of $TiB_2$ > TiB > Ti6Al4V was demonstrated by our theoretical and experimental investigations. These findings demonstrate that graded materials additive manufacturing is beneficial to fabricate metal-ceramic part successfully.

## Declaration of Competing Interest

The authors have declared that no conflict of interest exists.

## Acknowledgements

This work was supported by the National Natural Science Foundation of China (No. 51735005), and the National Key Research and Development Program (No. 2016YFB1100101).

## References

[1] C.Y. Yap, C.K. Chua, Z.L. Dong, Z.H. Liu, D.Q. Zhang, L.E. Loh, S.L. Sing, Appl. Phys. Rev. 2 (2015) 041101.
[2] H. Chen, D. Gu, D. Dai, M. Xia, C. Ma, Mater. Lett. 227 (2018) 128–131.
[3] C. Tan, K. Zhou, T. Kuang, Mater. Lett. 237 (2019) 328–331.
[4] J. Koopmann, J. Voigt, T. Niendorf, Metall. Mater. Trans. B. 50 (2019) 1042–1051.
[5] M. Kashtalyan, M. Menshykova, Compos. Struct. 87 (2009) 36–43.
[6] H. Chai, B. Lawn, J. Mater. Res. 15 (2000) 1017–1024.
[7] I. Shishkovsky, N. Kakovkina, V. Sherbakov, Compos. Struct. 169 (2017) 90–96.
[8] C. Cai, C. Radoslaw, J. Zhang, Q. Yan, S. Wen, B. Song, Y. Shi, Powder Technol. 342 (2019) 73–84.
[9] D. Sun, D. Gu, K. Lin, J. Ma, W. Chen, J. Huang, X. Sun, M. Chu, Powder Technol. 342 (2019) 371–379.
[10] H. Attar, M. Bönisch, M. Calin, L. Zhang, S. Scudino, J. Eckert, Acta Mater. 76 (2014) 13–22.
[11] L.Y. Chen, J.C. Huang, C.H. Lin, S.Y. Chen, T.L. Yang, D.Y. Lin, H.K. Lin, J.S.C. Jang, Mater. Sci. Eng. A. 682 (2017) 389–395.
[12] W. Xue, C. Wang, R. Chen, Z. Deng, Mater. Lett. 52 (2002) 435–441.